

Rock visualization using micro-CT scanner and X-ray transparent triaxial apparatus

M. Soldal¹, H. D. Wilkinson¹, I. Viken¹ and G. Sauvin¹.

The Norwegian Geotechnical Institute, Sognsveien 72, 0806 Oslo, Norway.

This paper was prepared for presentation at the International Symposium of the Society of Core Analysts held in Vienna, Austria, 27 August -1 September 2017

ABSTRACT

The macroscopic deformation and failure of rocks under compression is typically an gradual process of damage accumulation, crack formation and finally failure. Most often failure is accompanied by localization of deformation, which influence the stress distribution within the rock, and reduces its mechanical performance. Localization of strain in rock samples mechanically tested in the lab, can often take place unnoticed by deformation sensors. In this study a recently developed X-ray transparent triaxial test setup for rock testing inside a Computed Tomography (CT) scanner is utilized for the first time. Two different sandstones are scanned at progressively increasing shear stresses, enabling visualization of deformation taking place inside the sample as it is loaded to macroscopic failure.

INTRODUCTION

Experimental geomechanical investigation of rock deformation under varying stresses typically deals with global measurements of changing sample dimensions. However, most geomaterials exhibit strain localization into narrow zones when stressed, which may or may not be detectable using traditional deformation measurements. Strain localization under shear stress application typically indicates that failure is imminent [8], and the behaviour of bands with localized deformation can strongly influence the macroscopic response of the rock specimens, and should be investigated [3].

Various experimental measuring techniques have already been utilized in efforts to capture strain localization (e.g. acoustic techniques, microscopy, photogrammetry and multiple local strain measurements). One inherent challenge is that the necessary resolution and volume of interest can change rapidly, from the sample scale to narrow bands of strain

localization [4] and the measuring technique should capture all. One powerful tool for accessing the interior of rock samples and characterizing the density distribution within in a non-destructive manner is X-ray imaging. A given number of 2D projections of the sample in interest captured at various angles are used to reconstruct 3D volumes in X-ray Computed Tomography (CT). The CT volumes show the three-dimensional distribution of the sample's X-ray linear attenuation coefficient, which is closely related to the density [9].

Several intriguing studies of the onset of deformation localization as seen in a CT scanner are already available (e.g. [2,5, 7 and 8]). Most of them consider relatively small samples under low stresses. Others have shown deformational trends on more competent rocks by CT imaging samples prior to and after they are subjected to high shear stresses (e.g. [3]).

In this study, a newly developed X-ray transparent triaxial apparatus is utilized to isotropically consolidate (effective stress 5 MPa) and then shear 1.5" diameter samples. The apparatus enables 4D visualization of rock damage during destructive tests (i.e. during application of shear stresses). Here we describe the experimental equipment and present some results from drained triaxial tests on two different sandstones.

MATERIAL AND METHOD

CT scanner

A Nikon Metrology XT H 225 LC industrial CT scanner with a 225 kV micro-focus X-ray tube and a 4.2 Megapixels detector panel is used for imaging. The spot size of the X-ray beam is typically 3 μm . During a CT scan the object in interest rests on a manipulator table that rotates 360 degrees around its longitudinal axis. During this rotation, a specific number of 2D projections are collected and later turned into a 3D volume using some back-projection algorithms.

Optimization of settings to employ during CT acquisition can be a time-consuming task. The overall trade-off in this study is between time and image quality. Number of projections, frames to average, exposure time etc are all parameters that can enhance the signal to noise ratio, but also at the same time increase the acquisition time.

Artefacts in CT data can affect the result considerably. Most pronounced in this study are the ring artefacts. Ring artefacts are caused by defective pixel elements and show up as rings in the reconstructed CT volumes. The option of minimizing ring artefacts given by the acquisition software undertakes a process of shifting the projection images a specific number of pixels when collecting the CT data. As a result, the total acquisition time is significantly increased and it was decided to rather remove the ring artefacts in the image post processing. A method similar to that of Sijbers was utilized for this purpose [1], and an example of ring artefact removal is given in Figure 1.

Tracking the deformation field within the scanned rock volume as stress varies, involves several processing steps. Using both an in-house developed Matlab code and third-party Matlab code, the process consists of firstly defining a region of interest within the volume and a center of rotation. Afterwards the volume is processed and among other things, the ring artefacts are removed. The process of finding the displacement field involves subdividing the CT volumes iteratively into finer and finer sub-volumes, and for every refinement, the sub-volumes are phase-correlated to find the relative offset.

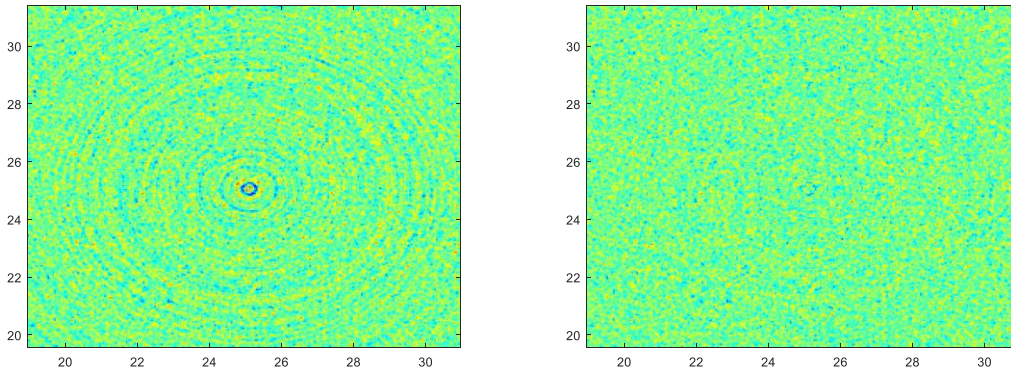


Figure 1: Color coded horizontal cross section of a CT scanned sandstone before (left) and after (right) ring artefact removal.

For each CT scan 3000 projections is collected, each taken using an exposure time of 1000ms. The time it takes to complete one scan is approximately 50 minutes, and the resulting voxel resolution is 45 μm .

Triaxial apparatus

The main challenge in designing the triaxial apparatus was the need for both X-ray transparency and sufficient system strength and stiffness. Our triaxial apparatus is self-compensating, meaning that there is no need for steel bars disturbing the X-rays to hold the top and bottom parts together and that the tensional axial forces are sustained by the cell body (see Figure 2). The cell body is mainly made up of winded carbonfiber with titanium end caps out of view for the CT image. In addition, an aluminum liner on the inside of the carbonfiber cylinder is absorbing some of the forces acting on the cell body. The axial force (up to 100 kN) is hydraulic applied through a piston connected to the bottom of the sample and controlled by a pressure controller. The top cap is equipped with bayonet fittings and securely attached to the titanium end piece. The top and bottom pieces have pore pressure inlets connected to pressure controllers, and stacked piezo ceramic elements for acoustic P, S1 and S2 measurements. The rock sample is enclosed in a rubber membrane which is surrounded by hydraulic oil enabling application of confining pressure using yet another pressure controller. Radial deformation is measured as the change in diameter at mid-height by a cantilever connected to the membrane. Axial deformation is measured by two LVDTs fixed to the top and bottom pieces.

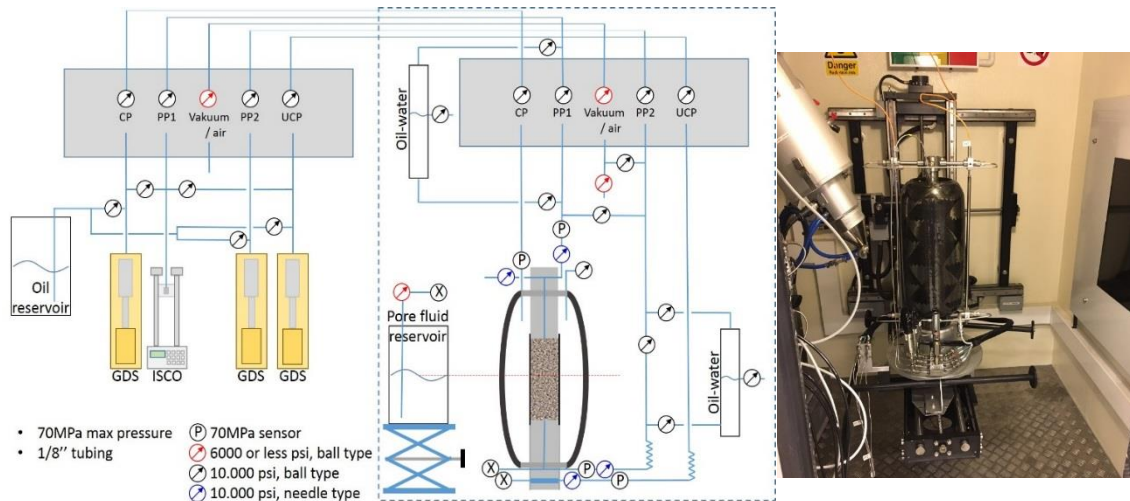


Figure 2: Schematics of the triaxial setup (left). The parts inside the dotted square are placed inside the CT cabinet, whereas the rest of the system is outside. To the right is an image of the X-ray transparent triaxial cell placed on the rotating manipulator table inside the cabinet.

On the X-rays' journey from the X-ray tube to the detector panel, they consequently have to pass through carbonfiber, aluminum, hydraulic oil, rubber membrane and rock sample. As the latter is the only object of interest, the rest are merely acting as filters causing an increased X-ray energy demand.

To accommodate the 360 degrees rotation of the triaxial apparatus during CT acquisition, flexible tubings are installed which can tolerate the rotation even at high pressures. As pressure controllers are located outside the CT cabinet and pressure drop in tubings are a function of their length, special care is taken to locate pressure transducers as close to the rock sample as possible.

Material

In this study, we give the results from two drained triaxial tests on two different sandstones (Figure 3). They were selected to represent different properties in terms of porosity, strength and deformation characteristics. Sample number 1 is a moderately layered sandstone with a porosity around 20 %, and it was drilled parallel with layering. Sample number 2 is a much weaker sandstone with a porosity of about 60 %. Both samples are approximately 38 mm in diameter and twice the diameter in height.



Figure 3: Sample number 1 (left) and sample number 2 (right) before triaxial testing.

Experimental procedure

After weighing and measuring the samples' diameters and heights, they are inserted into the triaxial cell. The piston and the top piece are brought in contact with the sample and the isotropic stress is increased to 1.0 MPa. Sample number 1 is saturated with brine at this effective stress and the backpressure is increased to 1 MPa. Sample number 2 is tested in dry conditions. Both samples are loaded isotropically to an effective stress of 5 MPa. This stress level serve as the reference level for further strains during the application of shear stresses.

Next, the effective vertical stress is increased in steps under drained conditions, while the horizontal effective stress is kept constant. After each step, the sample is allowed some time to stabilize before the CT acquisition begins. As progressively more shear stress and resulting strain is applied to the samples, it becomes impractical to ensure sample stabilization prior to CT acquisition. Most likely, this results in some image distortions in the later CT scans as the sample is deforming during CT scanning. Shear stress is increased until the sample fails or until further axial deformation can potentially damage the rubber membrane. Throughout the entire tests, all pressures and deformations are recorded.

RESULTS

Plots of shear stress versus axial strain for the two samples are given in Figure 4, together with the relative time for the CT acquisitions. Axial strain is given as the deformation recorded by the LVDTs divided by the initial sample height at the start of shearing and positive strain indicates compression. Sample number 1 displayed a relatively brittle behaviour, whereas sample number 2 displayed apparent strain hardening and did not lose its ability to withstand increasing shear stress. The reduction in shear stress in Figure 4 is from axial unloading to isotropic stress conditions before the final CT scan.

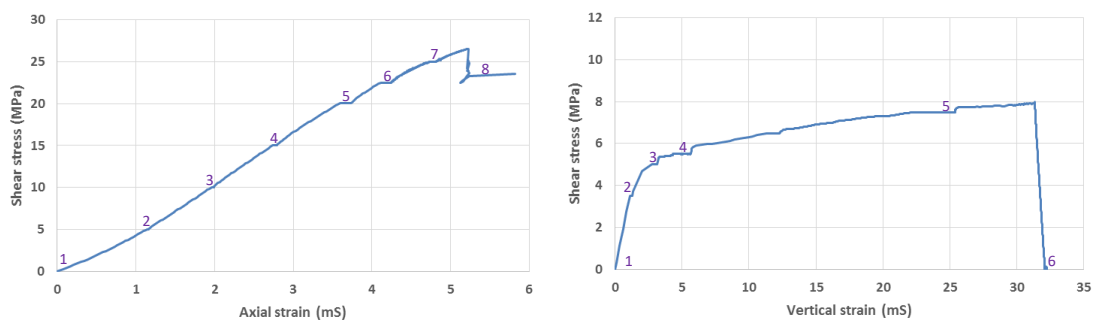


Figure 4: Axial strain versus shear stress for sample number 1 and 2. Numbers in purple indicate the relative timing of the CT scans.

Figure 5 shows the middle vertical cross section of sample 1 after it failed (left). The middle and right plots in fig 5 show the vertical displacement relative to the isotropic stress level before shearing. The displacement vectors indicate a downward movement of the upper right side of the failure plane.

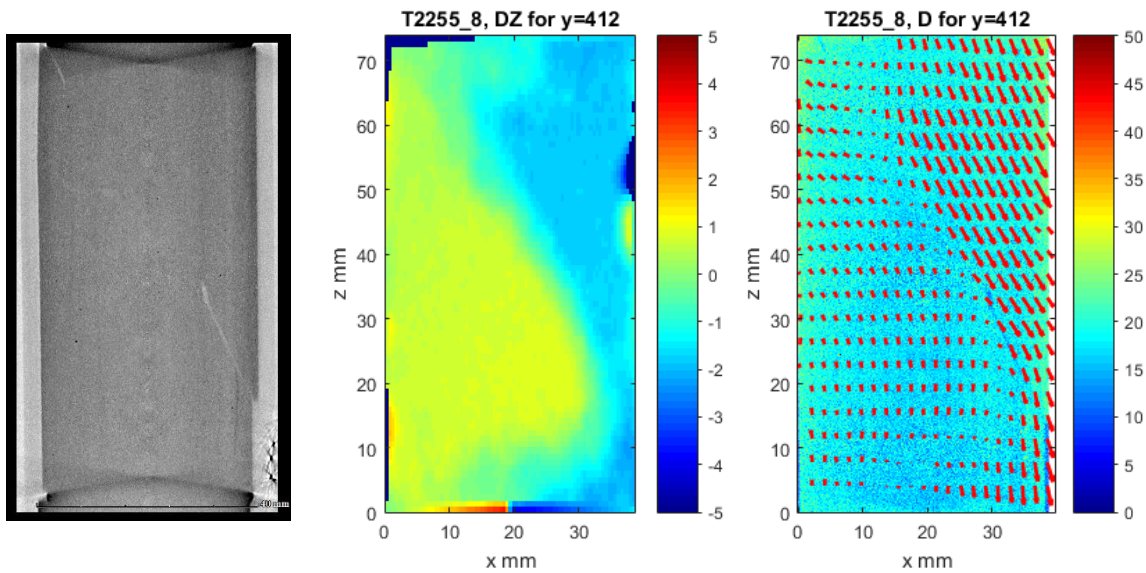


Figure 5: The central cross section of sample number 1 after macroscopic failure (left), the calculated relative displacement (middle) and the displacement vectors in the longitudinal axis (right). The processed volume is downscaled 4^3 times relative to the CT volume, and the displacement vectors are not to scale.

Sample 2 experienced compaction without ever forming a clear shear plane. The radial deformation sensor indicated only minor radial dilatation for sample 2 (approximately 1 mS). However, the CT images clearly show the occurrence of radial expansion in the lower 30 % or so of the sample (i.e. along diameters not recorded by the deformation sensor). Figure 6 shows the radial strain distribution along the middle vertical cross section from the CT scans. It is calculated from the reconstructed volumes' change in diameter with increasing shear stress.

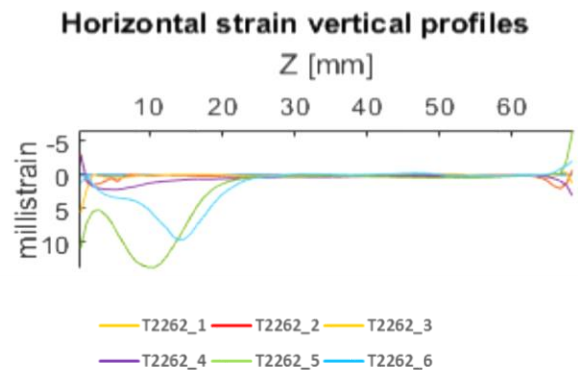


Figure 6: Radial strain calculated along the same vertical profile for the 6 CT scans of sample 2.

The central vertical cross sections from four CT scans for sample number 2 are given in Figure 7 (scans 3-6). The lower part of figure 7 shows the relative vertical displacement vectors for the same CT scans. With progressively increasing shear stress, the vertical deformation follows the radial deformation trend and concentrates in the lower region of the sample.

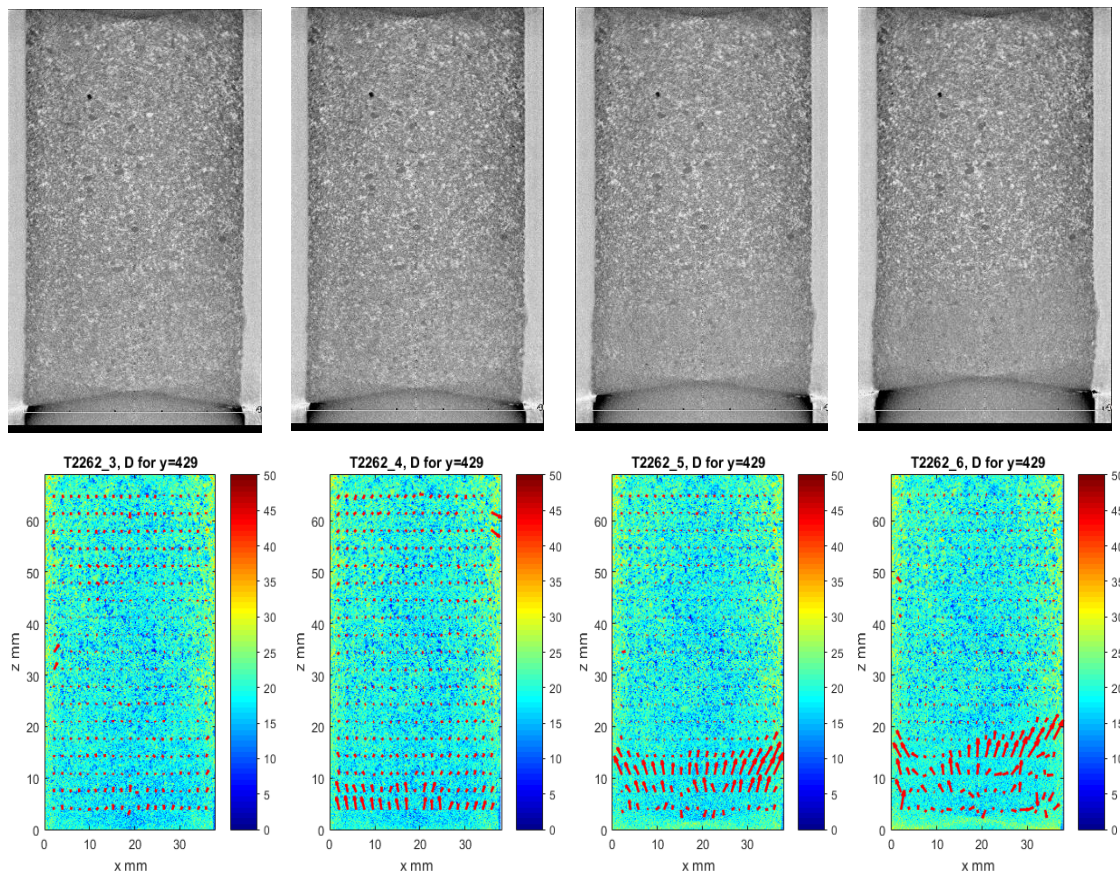


Figure 7: Vertical cross sections of CT scan 3-6 of sample 2 (top). The lower plot shows the calculated vertical displacement vectors in approximately the same cross sections.

CONCLUSION

Triaxial testing of normally sized samples under realistic reservoir conditions inside an industrial CT scanner inherently creates challenges in terms of image quality. Noise issues have to be addressed, and the material making up the triaxial cell body will absorb significant portions of the X-ray energy. Consequently, the exposure time and total acquisition time is increased. Even so, the opportunity of glancing into the rock interior as it deforms can increase the understanding of strain localization and distribution. In this study, with only preliminary data treatment of the first experiments in a new setup, we have seen that the

CT images can reveal deformation information not readily available using more traditional deformation sensors.

Experimental plans include coupling measurement of changes in geophysical properties (electrical and acoustic) directly to rock damage. Furthermore, the triaxial apparatus will be used to study fluid flow and porosity development under anisotropic stress conditions in various rocks. By combining measurements of changes in geophysical properties with detailed mapping of fluid saturation, the aim is to contribute to relevant rock models [1].

REFERENCES

- [1] Alemu, B. L., Aker, E., Soldal, M., Johnsen, Ø. and Aagard, P. Effect of sub-core scale heterogeneities on acoustic and electrical properties of a reservoir rock: a CO₂ flooding experiment of brine saturated sandstone in a computed tomography scanner. *Geophysical Prospecting*, (2013) **61**, 235-250.
- [2] Alikarami, R. and Torabi, A. Micro-texture and petrophysical properties of dilation and compaction shear bands in sand. *Geomechanics for Energy and the Environment*, (2015) **3**, 1-10.
- [3] Bèsuelle, P., Desrues, J. and Raynaud, S. Experimental characterisation of the localisation phenomenon inside a Vosges sandstone in a triaxial cell. *International Journal of Rock Mechanics & Mining Sciences*, (2000) **37**, 1223-1237.
- [4] Bèsuelle, P., Viggiani, G., Lenoir, N., Desrues, J. and Bornert, M. X-ray Micro CT for Studying Strain Localization in Clay Rocks under Triaxial Compression in *Advances in X-ray Tomography for Geomaterials*, ISTE, London (2006), 35-52.
- [5] Desrues, J. and Viggiani, G. Strain localization in sand: an overview of the experimental results obtained in Grenoble using stereophotogrammetry. *International Journal for Numerical and Analytical Methods in Geomechanics*, (2004) **28**, 279–321.
- [6] David, C., Menéndez, B. and Mengus, J. Influence of mechanical damage on fluid flow patterns investigated using CT scanning imaging and acoustic emissions techniques. *Geophysical Research Letters*, (2008) **35**, L16313.
- [7] Higo, Y. Oka, F., Kimoto, S., Sanagawa, T. and Matsushima, Y. Study of strain localization and microstructural changes in partially saturated sand during triaxial tests using microfocus X-ray CT. *Soils and Foundations*, (2011) **51**, 95–111.
- [8] Higo, Y., Oka, F., Sato, T., Matsushima, Y. and Kimoto, S. Investigation of localized deformation in partially saturated sand under triaxial compression using

- microfocus X-ray CT with digital image correlation. *Soils and Foundations*, (2013) **53**, 181-198.
- [9] Louis, L., Wong, T. and Baud, P. "Imaging strain localization by X-ray radiography and digital image correlation: Deformation bands in Rotbach sandstone. *Journal of Structural Geology*, (2007) **29**, 129-140.
- [10] Sijbers, J. and Postnov, A. Reduction of ring artefacts in high resolution micro-CT reconstructions. *Physics in Medicine and Biology*, (2004) **49**, 247-253.